

Using structural analysis *in silico* to assess the impact of missense variants in MEN1

Richard C. Caswell, Martina M. Owens, Adam C. Gunning, Sian Ellard, and
Caroline F. Wright

Journal of the Endocrine Society
Endocrine Society

Submitted: July 11, 2019
Accepted: September 20, 2019
First Online: September 27, 2019

Advance Articles are PDF versions of manuscripts that have been peer reviewed and accepted but not yet copyedited. The manuscripts are published online as soon as possible after acceptance and before the copyedited, typeset articles are published. They are posted "as is" (i.e., as submitted by the authors at the modification stage), and do not reflect editorial changes. No corrections/changes to the PDF manuscripts are accepted. Accordingly, there likely will be differences between the Advance Article manuscripts and the final, typeset articles. The manuscripts remain listed on the Advance Article page until the final, typeset articles are posted. At that point, the manuscripts are removed from the Advance Article page.

DISCLAIMER: These manuscripts are provided "as is" without warranty of any kind, either express or particular purpose, or non-infringement. Changes will be made to these manuscripts before publication. Review and/or use or reliance on these materials is at the discretion and risk of the reader/user. In no event shall the Endocrine Society be liable for damages of any kind arising references to, products or publications do not imply endorsement of that product or publication.

In silico structural analysis of *MEN1* variants

Using structural analysis *in silico* to assess the impact of missense variants in *MEN1*

Richard C. Caswell (1), Martina M. Owens (2), Adam C. Gunning (1), Sian Ellard (2) & Caroline F. Wright (1).

1: Institute of Biomedical and Clinical Science, University of Exeter School of Medicine, Exeter, United Kingdom. 2: Department of Molecular Genetics, Royal Devon & Exeter NHS Foundation Trust, Exeter, United Kingdom.

ORCID numbers:

0000-0002-2081-0188

Owens

Martina M

0000-0002-7620-5526

Ellard

Sian

0000-0003-2958-5076

Wright

Caroline F

0000-0003-0713-4602

Caswell

Richard C

Received 11 July 2019. Accepted 20 September 2019.

Key words: Multiple Endocrine Neoplasia type 1; protein structure; missense variant interpretation; genomics

Despite the rapid expansion in recent years of databases reporting either benign or pathogenic genetic variation, the interpretation of novel missense variants can remain challenging, particularly for clinical or genetic testing laboratories where functional analysis is often unfeasible. Previous studies have shown that thermodynamic analysis of protein structure *in silico* can discriminate between groups of benign and pathogenic missense variants. However, although structures exist for many human disease-associated proteins, such analysis remains largely unexploited in clinical laboratories. Here, we analysed the predicted effect of 338 known missense variants on the structure of menin, the *MEN1* gene product. Results provided strong discrimination between pathogenic and benign variants, with a threshold of >4 kcal/mol for the predicted change in stability providing a strong indicator of pathogenicity. Subsequent analysis of 7 novel missense variants identified during clinical testing of *MEN1* patients showed that all 7 were predicted to destabilise menin by >4 kcal/mol. We conclude that structural analysis provides a useful tool in understanding the

impact of missense variants in *MEN1*, and that integration of proteomic with genomic data could potentially contribute to the classification of novel variants in this disease.

INTRODUCTION

The rapid expansion in recent years of genomic data from both patient and control groups has vastly improved the quantity and quality of information that is available to clinicians in attempting to classify novel genetic variants. While it is often straightforward to interpret likely loss-of-function variants such as stop-gain or frameshift variants, the same is not true of missense variants, where the effect of an amino acid substitution is likely to be specific to its context in the protein of interest. Moreover, such variants are often rare or unique, and thus must be interpreted on a case-by-case basis.

Numerous methods have been developed for predicting the phenotypic effect of missense variants. As has been comprehensively reviewed elsewhere (1), these methods rely either on analysis of DNA and protein conservation, protein structure-based analysis, or a combination of the two. In the case of the latter, widely used tools such as PolyPhen are able to incorporate information on the nature of the amino acid change itself (e.g. Grantham distance between native and variant amino acids, changes in polarity or charge), effects on predicted secondary structure and, where available, data derived from the structural context, such as changes in hydrogen bonding or atomic crowding. However, such data is used in a qualitative, rule-based manner in the final prediction (1), and the tools which are most widely used in the clinical setting do not specifically address the quantitative effects of missense variants on protein stability. Nevertheless, these effects can be calculated where there is an experimental or modeled 3D structure for the protein of interest, and programs such as FoldX (2), Rosetta (3, 4) or other computational methods have been widely used by structural biologists to investigate the effects of missense variants on protein folding and stability (5, 6). Despite this, few studies have sought to address whether there is a direct clinical application of such an approach, i.e. whether pathogenic and benign variants can be distinguished on the basis of their predicted effects on thermodynamic stability.

The potential utility of protein stability data towards the analysis of missense variants has recently been demonstrated in studies of the Lynch syndrome protein, MSH2 (7), and in phenylalanine hydroxylase (PAH) (8), in which pathogenic variants result in phenylketonuria. Both these studies combined *in silico* analysis with extensive functional analysis of a number of MSH2 and PAH variants; however, resources for the latter are unlikely to be routinely available in clinical genetics laboratories. We have therefore asked whether *in silico* analysis, based predominantly on the predicted effects of missense variants on protein stability, can help discriminate between pathogenic and benign variation in the context of clinical testing of the *MEN1* gene.

Pathogenic variants in the *MEN1* gene cause Multiple Endocrine Neoplasia type I, an autosomal dominant disorder, in which patients develop neoplastic lesions in various endocrine tissues, principally the parathyroids, pituitary and pancreas (9). Pathogenic variants may either be inherited or acquired, but in both cases development of disease requires loss of heterozygosity consistent with a role for menin, the *MEN1* gene product, as a tumor suppressor. The biological activity of menin is not fully understood, but it is known to bind to and inhibit the activity of JunD (10), a component of the proliferation-associated transcription factor AP-1. Loss of menin activity is presumed to result in deregulated activity of AP-1, leading to increased cell proliferation and ultimately neoplasia. Menin also regulates gene expression via interaction with the histone methyltransferase KMT2A (MLL1), and forms an essential component of the MLL complex which upregulates expression from target genes including those of the *HOX* cluster (11). Menin may also play a role in DNA damage repair via an interaction with FANCD2, and loss of activity has been shown to result in increased

sensitivity to DNA damage (12). Finally, menin has been shown to repress telomerase activity, and depletion of menin in human fibroblasts results in their immortalization (13). Potentially therefore there are a number of pathways by which loss of menin activity could lead to neoplasia and tumor formation.

The most common presenting feature of MEN1 is hyperparathyroidism, which occurs in ~95% of patients due to tumors of the parathyroid gland; however, tumors are also frequently observed in the pancreatic islets (40-70%) and pituitary (30-40%) (14). Patients may also develop tumors of the adrenal cortex, carcinoid tumors and non-endocrine tumors, including lipomas, angiofibromas, collagenomas and meningiomas (15), resulting in a range of clinical symptoms which may overlap with other diseases of different genetic etiology (16-18). This overlap presents one of the key problems in assessing genetic variants in cases of MEN1. While a large number of pathogenic variants in *MEN1* have been reported, genetic testing continues to uncover novel missense substitutions which require assessment of their potential pathogenicity. A further confounding issue is the often later onset of disease, with reported age-related penetrance of 10-43% at 20 years and 81- 94% by 50 years (14, 19), which may lead to apparent non-segregation of a variant with disease within a family pedigree.

The identification of a genetic etiology has important implications for the patient and for their family members. With the exception of pituitary neuroendocrine tumors, MEN1-associated tumors are usually multiple and treatment is therefore challenging, requiring a multi-disciplinary team of experts to reduce morbidity and mortality (20). The identification of the familial disease-causing variant enables the identification of carriers when they are still asymptomatic. Clinical surveillance in these individuals allows early recognition of the clinical manifestations and therapeutic intervention. For example, primary hyperparathyroidism often remains asymptomatic in many patients but prolonged hypercalcemia usually results in bone loss and/or nephrocalcinosis (21).

Approximately 20% of the variants identified in the *MEN1* gene are missense variants (22). The standards and guidelines published by the American College of Medical Genetics and Genomics (ACMG) and the Association for Molecular Pathology (AMP) describe a framework for the classification of sequence variants (23). Adjustments to this framework for the interpretation of *MEN1* missense variants has been proposed (24). However both agree that variants of uncertain significance should not be used to guide the clinical management of patients. This could lead to an under-diagnosis of MEN1 and a lost opportunity for screening at-risk relatives. For these reasons, methods to assist the classification of variants in *MEN1* would be of clinical value. The availability of a number of experimental structures for menin, the *MEN1* gene product, raises the possibility that structural analysis may provide such clinical utility.

We report here that thermodynamic analysis of *MEN1* variants *in silico* provides a very strong positive predictive value for pathogenicity, thereby helping to assess the impact of novel missense variants on protein function and potentially allowing its use as an aid to variant classification, and discuss briefly the scope for wider application of this approach to other diseases.

MATERIALS & METHODS

Variant groups, transcripts and numbering.

Lists of previously-reported, inherited missense SNVs in *MEN1* were downloaded from the Human Gene Mutation Database, Professional version (HGMD Pro) (25), the Genome Aggregation Database (gnomAD) (26) and the Sydney Genomics Collaborative Database (SGCD) (27). For the purposes of this analysis, variants were divided into groups as follows: pathogenic: DM ('disease mutation') class variants reported in HGMD Pro but not in gnomAD or SGCD (n=162); benign: variants reported in gnomAD or SGCD but not as DM

class in HGMD Pro (n=206); uncertain: variants reported as DM in HGMD Pro and present in gnomAD and/or SGCD (n=14). Different nucleotide substitutions resulting in the same coding change were regarded as a single missense substitution. In addition to these previously-reported variants, analysis was performed on seven novel missense variants: H46P; A164P; L175P; A345P; I360F; F364S; and G419D (see Table 1 for details). These variants were identified in our laboratory as part of the NHS (England) Genetic Testing service for rare inherited diseases. The patients tested fulfilled the criteria for a clinical diagnosis of MEN1 (14), presenting with at least two out of the three main MEN1-associated endocrine lesions or one typical MEN1-associated tumour and a first-degree relative with MEN1 or MEN1-associated lesion at a young age. For patients with a family history, the relevant variants (H46P, A164P, I360F and F364S) were all shown to co-segregate with disease in the family. Informed consent for genetic testing was obtained from all subjects.

There is one major isoform (610 amino acids) and one minor isoform (615 amino acids) of menin in the sequence databases. The longer minor isoform could have originated by use of an alternative splice donor site in exon 1 such that the longer isoform contains 5 residues inserted at the end of exon 1 (at amino acid 148) that leads to a total 615 amino acid coding region. While gnomAD and SGCD variants are annotated according to the 615-residue isoform encoded by transcripts NM_130803/ENST00000337652, HGMD Pro and structural databases use the 610-residue isoform encoded by NM_130799/ENST00000312049 as default. All numbering in this manuscript refers to the 610-residue form of menin, and variants from gnomAD and SGCD have been re-annotated accordingly.

Protein structures.

Structures of human menin were downloaded as PDB files from the worldwide Protein Data Bank (28); a full list of the 29 crystal structures, containing 31 discrete menin chains, used in this analysis is shown in Table 2. Any non-native amino acids (e.g. affinity purification tags) in these structures were removed from PDB files prior to further analysis.

***In silico* mutagenesis and thermodynamic analysis.**

Prior to *in silico* mutagenesis, sidechain repair and energy minimization was performed on all 31 menin chains in isolation, using the RepairPDB function of the FoldX modeling suite (2), version 4. The FoldX BuildModel function was then used to introduce individual substitutions into each of the repaired PDB structures. Of the 389 unique missense variants, 338 were covered by at least one PDB structure (pathogenic, n=161; benign, n=161; uncertain, n=9; novel, n=7). For each substitution, FoldX reported a change in free energy ($\Delta\Delta G$) resulting from the substitution; from this, an average $\Delta\Delta G$ value was calculated for each variant across all structures containing the relevant position. In total, all 31 structures were used for 308/338 variants (mean for all variants = 29), whereas due to differences in coverage of individual PDB files, analysis was possible using only a single structure for 7 variants. A full list of variants, the number of PDB structures analysed for each and average $\Delta\Delta G$ values for each variant has been published online (37). All structures were visualized in PyMOL (38).

Calculation of solvent accessibility.

The absolute area accessible to solvent (ASA) was calculated on a residue-by-residue basis for 7 representative structures of menin using DSSP (39, 40) version 3.0.0 (41). After calculating an average ASA value for each residue, relative solvent accessibility (RSA) was derived using the theoretical scale described by Tien et al. (42). A list of structures used for DSSP analysis is included in Table 2.

RESULTS

Pathogenic variants in MEN1 are predicted to be more destabilising than benign variants.

Over 30 crystal structures have previously been reported for menin (e.g. Figure 1A); most of these contain the protein in isolation or bound to a small (drug) ligand, while others show menin in complex with peptides from JunD, KMT2A or PSIP (Figure 1B; Table 2). Although all structures have been derived from expression of full-length (or near full-length) menin, a number of regions remain unresolved in crystal structures. These regions predominantly lie in the C-terminal of the protein and correspond to stretches of predicted intrinsic disorder (43) in the protein (Figure 1C, D), presumably resulting in high mobility within crystals. Interestingly, while these regions contain a similar distribution of benign variants as that seen in the protein as a whole, inherited pathogenic variants are rare in regions of predicted disorder in menin (Figure 1D); however, we cannot rule out the possibility that the lack of pathogenic variants in these regions is due to reporting bias towards variants which lie close to those already known. Furthermore, recurrent missense variants have been observed in disordered regions of menin in the COSMIC database of somatic mutations in cancer (44), of which three (R479W, R485Q and P540R) have not been reported in gnomAD. It is possible therefore that missense variants in disordered regions play a role in pathogenicity, particularly when arising as somatic mutations. With respect to inherited pathogenic variants however, their distribution almost entirely within ordered regions means that the vast majority (161/162) are covered by one or more PDB entries and are thus amenable to structural analysis.

The overall structure of menin is highly comparable within all reported PDB structures (alignment to PDB 6b41 yields an average root-mean-square deviation, RMSD, of 0.65 Å; range 0.55-1.10 Å). Moreover, there is no significant effect of ligand binding on menin structure (Figure 2). Since different PDB files contain slightly different numbers of amino acids but there are no obvious structural outliers, all available structures were used for thermodynamic analysis of missense variants *in silico* using FoldX.

Benign and pathogenic variant groups were highly distinguishable by their predicted effect on thermodynamic stability, as represented by average $\Delta\Delta G$ value calculated across all structures. Variants resulting in $\Delta\Delta G > 3$ kcal/mol are generally regarded strongly destabilising (45). The average $\Delta\Delta G$ value for all pathogenic variants was 5.06 kcal/mol (SD, 4.25 kcal/mol), with 108/161 of these (67.1%) predicted to be strongly destabilizing ($\Delta\Delta G > 3$ kcal/mol). In contrast, the average $\Delta\Delta G$ value for putatively benign (gnomAD and SGCD) variants was 1.13 kcal/mol (SD, 1.46 kcal/mol), with only 17/161 (10.6%) having an effect in excess of 3 kcal/mol (Figure 3A). Notably, all seven novel missense variants were also predicted to be strongly destabilising (average $\Delta\Delta G$, 7.67 kcal/mol; SD 3.14 kcal/mol; range, 4.81-13.16 kcal/mol). Analysis of $\Delta\Delta G$ values for individual PDB structures showed a similar separation of putative benign and pathogenic variant groups, with the vast majority of variants falling into a similar range for all structures (Figure 3B). We further compared the effect at multi-allelic sites where different benign and pathogenic missense variants occur at the same position. Analysis of 27 benign and 23 pathogenic variants co-occurring at 22 residues again showed that the difference between the two groups was highly significant ($p = 0.0002$), and that as a group, pathogenic missense changes were more strongly destabilizing than benign ones at the same position (average $\Delta\Delta G$ value by group = 6.81 kcal/mol and 2.18 kcal/mol respectively) (Figure 3C). Therefore since both pathogenic and benign variation can occur at the same site within menin, it is important to consider both the position and nature of the amino acid change; this data suggests that $\Delta\Delta G$ value may provide a useful tool in assessing the impact of novel variants at multi-allelic sites.

If variants which destabilize menin structure do indeed have a greater tendency to be pathogenic, it might be expected that variants most frequently observed in the general population would have the least destabilizing effect. This appears to be the case, as variants with the highest population frequency had average predicted $\Delta\Delta G$ values in the range -1 to +1 (Figure 4); as the error in FoldX calculations is approximately ± 0.8 kcal/mol (2), this suggests little or no effect of these variants on protein stability. Notably, those variants which have also been observed in an aging healthy population, as represented by the SGCD cohort (median age, 80-85 years) and are therefore most likely to be truly benign, all occur within this range of $\Delta\Delta G$ values. This group includes the only commonly-occurring missense *MEN1* variant, R171Q, which has an average $\Delta\Delta G$ value of 0.15 kcal/mol. Conversely, we note that some variants reported in gnomAD have $\Delta\Delta G$ values >4 kcal/mol, and in fact 2/9 of these variants (S38P, D315Y) have also been reported as disease-causing in HGMD Pro. This may reflect the confounding effect of late onset of symptoms in *MEN1* on apparent constraint against coding variation, whereby some variants reported in gnomAD may in fact lead to disease in later life.

Most pathogenic variants are buried in the menin structure.

To examine whether there are differences in the spatial distribution of benign and pathogenic variants, we calculated the relative solvent accessibility (RSA) of wild-type residues at all positions of missense substitutions (37). This showed that while positions of benign variants are distributed throughout the volume of the protein, 86.3% of pathogenic variants occur in solvent-inaccessible (i.e. buried) regions of RSA <0.2 (Figure 5A). Notably, this is also true for the 7 novel variants, 6 of which had an RSA value <0.02 . Plotting RSA against $\Delta\Delta G$ showed that variants at buried positions were also likely to be the most strongly destabilizing to protein structure (Figure 5B). Nevertheless, we observed that a significant number of pathogenic variants exhibited both accessibility to solvent (RSA >0.2) and relatively low $\Delta\Delta G$. Mapping the positions of solvent-accessible variants onto the surface of menin showed that, as for distribution throughout the internal volume of the protein, benign variants tended to be distributed across the surface. In contrast, pathogenic variants appeared to occur in clusters, one of which corresponds to binding surfaces for JunD, KMT2A and PSIP (Figure 5C, D), while another occurs on the opposite surface of menin to the JunD binding pocket. It is possible therefore that the latter region represents the site of an as-yet uncharacterized functional interaction of menin. As described above, 6/7 novel missense variants occur at positions which are buried in the interior of the protein, whereas the only solvent-accessible variant, H46P, occurs at the interface with KMT2A and presumably acts to impair this interaction (Figure 5E).

To investigate the effects of protein interactions on the thermodynamic effects of *MEN1* variants further, we compared $\Delta\Delta G$ values for variants in PDB structure 3u88 (menin complexed with KMT2A and PSIP peptides) by analysis both of menin chains in isolation (chains A, B) and complexed to KMT2A and PSIP. As expected, regions of decreased solvent accessibility in the complexes aligned with residues annotated as forming protein-protein contacts (Figure 6). However, the presence of bound peptides had little effect on $\Delta\Delta G$ values of benign variants, indicating that these have a neutral effect on protein binding. Conversely, protein binding had a large effect on $\Delta\Delta G$ values of a number of pathogenic variants; again, these predominantly occurred at or close to protein interfaces, indicating that these variants are likely to have a direct effect on ligand binding by menin.

Destabilizing variants reduce levels of functional menin protein.

Previous reports studying the effects of missense variants on levels of functional menin within the cell have shown that pathogenic variants have a tendency to increase protein turnover and/or reduce the steady-state level of protein, while benign variants tend to have no

such effect (46, 47). We correlated the previously-reported effects of variants on levels of steady-state protein with average $\Delta\Delta G$ values, and observed that variants which were predicted to be strongly destabilizing *in silico* ($\Delta\Delta G > 3$ kcal/mol) exhibited significantly lower levels of steady-state protein in cell-based assays ($p=0.0001$, Figure 7), consistent with the hypothesis that variants with high $\Delta\Delta G$ values reduce the biological activity of menin.

Can $\Delta\Delta G$ value be used as an aid to variant classification?

To evaluate the clinical validity of $\Delta\Delta G$ values, we performed Receiver Operating Characteristic (ROC) curve analysis for the groups of benign and pathogenic variants and compared the results with the outputs from a number of commonly-used phenotypic predictions tools: SIFT (48), PolyPhen (49) and REVEL (50). All methods yielded areas under the curve (AUC) of 0.819-0.864, indicating that all have clinical validity (Figure 8A). However $\Delta\Delta G$ analysis resulted in the highest specificity but lowest sensitivity. Values of $\Delta\Delta G > 3$ kcal/mol are generally regarded as being strongly destabilizing towards protein structure (45); taking this as a threshold for variant classification gives sensitivity and specificity of 67.1% and 89.4% (positive predictive value, 86.4%), while setting a more conservative threshold of ≥ 4 kcal/mol increased the specificity to 95.0%, though with a concomitant loss of sensitivity (54.0%; positive predictive value, 90.6%). A marginal increase in positive predictive value (PPV) could be obtained by combining $\Delta\Delta G$ thresholds with a cut-off in the REVEL score of 0.7, which has been reported to exclude 95% of false positive calls (51), yielding PPV's of 87.7% at $\Delta\Delta G \geq 3$ kcal/mol and 91.5% at $\Delta\Delta G \geq 4$ kcal/mol. Notably, all seven novel missense variants reported here cluster within the upper right quadrant (Figure 8B), consistent with a severe impact on protein stability and suggesting that $\Delta\Delta G$ values can potentially be used to provide evidence towards variant classification in MEN1.

DISCUSSION

Previous work has shown that predicted thermodynamic destabilization of protein structure, as measured by $\Delta\Delta G$ values calculated by FoldX, can be used as a predictor of pathogenicity in *MSH2* and *PAH* variants (7, 8). Our data indicates that the same is true for variants in *MEN1*, and that a high predicted $\Delta\Delta G$ value is a strong positive predictor for pathogenicity. Using a threshold value of $\Delta\Delta G > 3$ kcal/mol, which is generally regarded as strongly destabilizing, yielded a specificity of 89.4% for classification of menin variants, rising to 95.0% for a more conservative threshold of 4 kcal/mol. By contrast, using a proposed threshold of 0.7 for the phenotypic meta-prediction tool REVEL yielded a specificity of only 53%. Although *MEN1* has a high degree of penetrance, with more than 95% expected to develop symptoms by the sixth decade of life (9), there appears to be no correlation between *MEN1* variants and clinical manifestations, with inter- and intra-familial variation observed (22). Therefore the identification of likely pathogenic variants has significant implications for patient surveillance and genetic testing of family members. For example, analysis of a large cohort of Florentine patients showed age at genetic diagnosis for relatives of the index cases as 31.2 ± 16.9 years, with a range of 1–71 years (21). With respect to the seven novel missense variants reported here, all had high average predicted $\Delta\Delta G$ values (range, 4.81–13.16 kcal/mol) and six were deeply buried within the protein, strongly supporting pathogenicity. All these cases were also predicted as deleterious or probably pathogenic by commonly-used tools for *in silico* pathogenicity prediction; however, the comparatively low specificity of all these tools for variants in *MEN1* highlights the value of thermodynamic analysis as a means of reducing false positive calls.

As might be expected, our analysis shows that variants which are buried within the menin structure are those that are predicted to result in greatest structural destabilization. In fact, the majority (86.3%) of reported germline pathogenic variants in *MEN1* are buried, suggesting that any novel variant which is solvent inaccessible ($RSA < 0.2$) and has a predicted $\Delta\Delta G > 4$ kcal/mol is also highly likely to be pathogenic. Nevertheless, a number of pathogenic variants lie on the surface of menin, and many of these have relatively low $\Delta\Delta G$ values. A number of these variants lie at or close to positions of known interactions with binding partners such as JunD, KMT2A or PSIP, where they presumably have an adverse effect on binding of these factors, emphasizing the value of integrating all known structural annotation into a final classification of the likely effect of a variant. Our data also suggests the possible existence of an as-yet unidentified interaction of menin, as evidenced by the cluster of pathogenic variants lying on the protein surface opposite the JunD binding pocket. Interestingly, in a recent analysis of the spatial distribution of missense variants (52), *MEN1* was identified as one of a group of genes displaying significant spatial clustering of pathogenic and likely pathogenic missense variants in the ClinVar database (53), but not of benign or likely benign missense variants reported in gnomAD. Inspection of ClinVar (accessed 19 September 2019) revealed that of 346 missense variants in *MEN1*, only 50 unique variants (excluding start-loss variants) were classified as pathogenic or likely pathogenic, with a large majority (276) classed as being of uncertain significance. Although we have used a different database, HGMD Pro, as the source for our dataset of ‘pathogenic’ variants, there is considerable overlap between the two, with 39/50 (78%) of the pathogenic or likely pathogenic ClinVar variants also being present in our dataset, while a further 27 variants in our dataset were colocalized with a ClinVar variant. However, the discrepancy between the total number of ‘pathogenic’ variants in the two datasets highlights the need for more reliable tools for classification of variants in *MEN1*.

In terms of broader applicability of this approach, our work builds upon the reported analysis of *MSH2* and *PAH* variants and applies it to the classification of novel clinical variants. Whether the same approach can be used for other proteins remains to be determined. One obvious limitation of structural analysis is, by definition, the need for a suitable structural model. However, even where no experimental structures are available for a protein of interest, it may still be possible to use comparative modelling to generate a reliable model of regions or domains which can be used for structural analysis. Another likely limitation is the architecture of the protein itself. Both menin and *MSH2* are relatively compact, globular proteins, with low surface area to volume ratio and a high proportion of amino acids in regions of secondary structure. As a result, the effect of missense variants on the internal geometry and thermodynamic stability of the proteins is amenable to *in silico* prediction, particularly given the availability of suitable high-quality PDB structures. It seems likely therefore that the approach used here may have broader applicability in proteins which contain a high proportion of buried residues in regions of strong secondary structure; indeed, the potential for wider use of *in silico* thermodynamic analysis of protein stability as part of a pipeline for assessing the impact of missense variants has recently been reviewed (54). However, less well-structured proteins, or fibrillar proteins where a greater proportion of amino acids are exposed to solvent, are likely to be less amenable to such study as the confidence with which the structural and thermodynamic effects of missense variants can be predicted will be greatly reduced. Such rules are likely to be revealed only by proteome-wide study which is beyond the scope of this manuscript.

In summary, we have shown that structural analysis of missense substitutions in *MEN1* can be used to identify variants likely to destabilize the protein and thus potentially as an aid in variant classification. Given that all analysis described herein used publicly-available data, freely-available software and does not require specialist bioinformatic skills or infrastructure,

such analysis lies within the capability of any genetics laboratory or testing service. As such, there is significant scope to make greater use of protein structural data in the routine interpretation of genetic variation.

ACKNOWLEDGMENTS

The authors wish to acknowledge support from the Wellcome Trust (grant no. 200990).

Financial support: This work was supported by the Wellcome Trust (grant no. 200990).

Wellcome Trust <http://dx.doi.org/10.13039/100004440>, 200990, Sian Ellard

Corresponding author (to whom reprint requests should be addressed): Richard C Caswell; email: r.caswell@exeter.ac.uk; tel: +44 1392 408506

Disclosure statement:

All authors declare that they have no competing interests.

DATA AVAILABILITY

All data generated or analysed during this study are included or cited in this published article, with the exception of $\Delta\Delta G$ and RSA values calculated from individual PDB structures and subsequently used to calculate average values for each variant (38). This data is available from the corresponding author on reasonable request.

REFERENCES

1. Tang H, Thomas PD. Tools for Predicting the Functional Impact of Nonsynonymous Genetic Variation. *Genetics* 2016;203(2):635-647.
2. Schymkowitz J, Borg J, Stricher F, Nys R, Rousseau F, Serrano L. The FoldX web server: an online force field. *Nucleic Acids Res.* 2005;33(Web Server issue):W382-388.
3. Kellogg EH, Leaver-Fay A, Baker D. Role of conformational sampling in computing mutation-induced changes in protein structure and stability. *Proteins* 2011;79(3):830-838.
4. Leaver-Fay A, Tyka M, Lewis SM, Lange OF, Thompson J, Jacak R, Kaufman K, Renfrew PD, Smith CA, Sheffler W, Davis IW, Cooper S, Treuille A, Mandell DJ, Richter F, Ban YE, Fleishman SJ, Corn JE, Kim DE, Lyskov S, Berrondo M, Mentzer S, Popović Z, Havranek JJ, Karanicolas J, Das R, Meiler J, Kortemme T, Gray JJ, Kuhlman B, Baker D, Bradley P. ROSETTA3: an object-oriented software suite for the simulation and design of macromolecules. *Methods Enzymol.* 2011;487:545-574.
5. Compiani M, Capriotti E. Computational and theoretical methods for protein folding. *Biochemistry* 2013;52(48):8601-8624.
6. Masso M, Vaisman II. AUTO-MUTE: web-based tools for predicting stability changes in proteins due to single amino acid replacements. *Protein Eng Des Sel.* 2010;23(8):683-687.
7. Nielsen SV, Stein A, Dinitzen AB, Papaleo E, Tatham MH, Poulsen EG, Kassem MM, Rasmussen LJ, Lindorff-Larsen K, Hartmann-Petersen R. Predicting the impact of Lynch syndrome-causing missense mutations from structural calculations. *PLoS Genet.* 2017;13(4):e1006739.
8. Scheller R, Stein A, Nielsen SV, Marin FI, Gerdes AM, Di Marco M, Papaleo E, Lindorff-Larsen K, Hartmann-Petersen R. Toward mechanistic models for genotype-phenotype correlations in phenylketonuria using protein stability calculations. *Hum Mutat.* 2019;40(4):444-457.
9. Lemos MC, Thakker RV. Multiple endocrine neoplasia type 1 (MEN1): analysis of 1336 mutations reported in the first decade following identification of the gene. *Hum Mutat.* 2008;29(1):22-32.

10. Argawal SK, Guru SC, Heppner C, Erdos MR, Collins RM, Park SY, Saggari S, Chandrasekharappa SC, Collins FS, Spiegel AM, Marx SJ, Burns AL. Menin interacts with the AP1 transcription factor JunD and represses JunD-activated transcription. *Cell*. 1999;96(1):143-152.
11. Yokoyama A, Wang Z, Wysocka J, Sanyal M, Aufiero DJ, Kitabayashi I, Herr W, Cleary ML. Leukemia proto-oncoprotein MLL forms a SET1-like histone methyltransferase complex with menin to regulate *Hox* gene expression. *Mol Cell Biol*. 2004, 24(13):5639-5649.
12. Jin S, Mao H, Schnepf RW, Sykes SM, Silva AC, D'Andrea AD, Hua X. Menin associates with FANCD2, a protein involved in repair of DNA damage. *Cancer Res*. 2003, 63(14):4204-4210.
13. Lin SY, Elledge SJ. Multiple tumor suppressor pathways negatively regulate telomerase. *Cell*. 2003, 113(7):881-889.
14. Thakker RV, Newey PJ, Walls GV, Bilezikian J, Dralle H, Ebeling PR, Melmed S, Sakurai A, Tonelli F, Brandi ML; Endocrine Society. Clinical practice guidelines for multiple endocrine neoplasia type 1 (MEN1). *J Clin Endocrinol Metab*. 2012;97(9):2990-3011.
15. Ellard S, Hattersley AT, Brewer CM, Vaidya B. Detection of a *MEN1* gene mutation depends on clinical features and supports current referral criteria for diagnostic molecular genetic testing. *Clin Endocrinol (Oxf)*. 2005;62(2):169-175.
16. Alberto F. Genetics of parathyroid disorders: Overview. *Best Pract Res Clin Endocrinol Metab*. 2018;32(6):781-790.
17. Beckers A, Aaltonen LA, Daly AF, Karhu A. Familial isolated pituitary adenomas (FIPA) and the pituitary adenoma predisposition due to mutations in the aryl hydrocarbon receptor interacting protein (AIP) gene. *Endocr Rev*. 2013;34(2):239-277.
18. Kövesdi A, Tóth M, Butz H, Szücs N, Sárman B, Pusztai P, Tőke J, Reismann P, Fáklya M, Tóth G, Somogyi A, Borka K, Erdei A, Nagy EV, Deák V, Valkusz Z, Igaz P, Patócs A, Grolmusz VK. True MEN1 or phenocopy? Evidence for geno-phenotypic correlations in MEN1 syndrome. *Endocrine* 2019;65(2):451-459.
19. Schaaf L, Pickel J, Zinner K, Hering U, Höfler M, Goretzki PE, Spelsberg F, Raue F, von zur Mühlen A, Gerl H, Hensen J, Bartsch DK, Rothmund M, Schneyer U, Dralle H, Engelbach M, Karges W, Stalla GK, Höppner W. Developing effective screening strategies in multiple endocrine neoplasia type 1 (MEN 1) on the basis of clinical and sequencing data of German patients with MEN 1. *Exp Clin Endocrinol Diabetes*. 2007;115(8):509-517.
20. Thakker RV. Multiple endocrine neoplasia type 1 (MEN1) and type 4 (MEN4). *Mol Cell Endocrinol*. 2014;386(1-2):2-15.
21. Marini F, Giusti F, Brandi ML. Multiple endocrine neoplasia type 1: extensive analysis of a large database of Florentine patients. *Orphanet J Rare Dis*. 2018;13(1):205.
22. Concolino P, Costella A, Capoluongo E. Multiple endocrine neoplasia type 1 (MEN1): An update of 208 new germline variants reported in the last nine years. *Cancer Genet*. 2016;209(1-2):36-41.
23. Richards S, Aziz N, Bale S, Bick D, Das S, Gastier-Foster J, Grody WW, Hegde M, Lyon E, Spector E, Voelkerding K, Rehm HL; ACMG Laboratory Quality Assurance Committee. Standards and guidelines for the interpretation of sequence variants: a joint consensus recommendation of the American College of Medical Genetics and Genomics and the Association for Molecular Pathology. *Genet Med*. 2015;17(5):405-424.
24. Romanet P, Odou MF, North MO, Saveanu A, Coppin L, Pasmant E, Mohamed A, Goudet P, Borson-Chazot F, Calender A, Bérout C, Lévy N, Giraud S, Barlier A. Proposition of adjustments to the ACMG-AMP framework for the interpretation of *MEN1* missense variants. *Hum Mutat*. 2019;40(6):661-674.

25. Stenson PD, Mort M, Ball EV, Evans K, Hayden M, Heywood S, Hussain M, Phillips AD, Cooper DN. The Human Gene Mutation Database: towards a comprehensive repository of inherited mutation data for medical research, genetic diagnosis and next-generation sequencing studies. *Hum Genet.* 2017;136(6):665-677. <https://portal.biobase-international.com/cgi-bin/portal/>. Accessed October 25 2018.
26. gnomAD (The Genome Aggregation Database). Cambridge, MA: Broad Institute, 2018. <https://gnomad.broadinstitute.org>. Accessed October 25 2018.
27. Sydney Genomics Collaborative Database. Sydney, Australia: Garvan Institute of Medical Research, 2018. <https://sgc.garvan.org.au>. Accessed October 25 2018.
28. wwPDB consortium. Protein Data Bank: the single global archive for 3D macromolecular structure data. *Nucleic Acids Res.* 2019;47(Database issue):D520-D528. <http://www.wwpdb.org>. Accessed October 25 2018.
29. Huang J, Gurung B, Wan B, Matkar S, Veniaminova NA, Wan K, Merchant JL, Hua X, Lei M. The same pocket in menin binds both MLL and JUND but has opposite effects on transcription. *Nature.* 2012;482(7386):542-546.
30. Shi A, Murai MJ, He S, Lund G, Hartley T, Purohit T, Reddy G, Chruszcz M, Grembecka J, Cierpicki T. Structural insights into inhibition of the bivalent menin-MLL interaction by small molecules in leukemia. *Blood.* 2012; 120(23):4461-4469.
31. Zhou H, Liu L, Huang J, Bernard D, Karatas H, Navarro A, Lei M, Wang S. Structure-based design of high-affinity macrocyclic peptidomimetics to block the menin-mixed lineage leukemia 1 (MLL1) protein-protein interaction. *J Med Chem.* 2013;56(3):1113-1123.
32. He S, Senter TJ, Pollock J, Han C, Upadhyay SK, Purohit T, Gogliotti RD, Lindsley CW, Cierpicki T, Stauffer SR, Grembecka J. High-affinity small-molecule inhibitors of the menin-mixed lineage leukemia (MLL) interaction closely mimic a natural protein-protein interaction. *J Med Chem.* 2014;57(4):1543-1556.
33. Borkin D, He S, Miao H, Kempinska K, Pollock J, Chase J, Purohit T, Malik B, Zhao T, Wang J, Wen B, Zong H, Jones M, Danet-Desnoyers G, Guzman ML, Talpaz M, Bixby DL, Sun D, Hess JL, Muntean AG, Maillard I, Cierpicki T, Grembecka J. Pharmacologic inhibition of the Menin-MLL interaction blocks progression of MLL leukemia in vivo. *Cancer Cell.* 2015;27(4):589-602.
34. Borkin D, Pollock J, Kempinska K, Purohit T, Li X, Wen B, Zhao T, Miao H, Shukla S, He M, Sun D, Cierpicki T, Grembecka J. Property Focused Structure-Based Optimization of Small Molecule Inhibitors of the Protein-Protein Interaction between Menin and Mixed Lineage Leukemia (MLL). *J Med Chem.* 2016;59(3):892-913.
35. Pollock J, Borkin D, Lund G, Purohit T, Dyguda-Kazimierowicz E, Grembecka J, Cierpicki T. Rational Design of Orthogonal Multipolar Interactions with Fluorine in Protein-Ligand Complexes. *J Med Chem.* 2015;58(18):7465-7474.
36. Xu S, Aguilar A, Xu T, Zheng K, Huang L, Stuckey J, Chinnaswamy K, Bernard D, Fernández-Salas E, Liu L, Wang M, McEachern D, Przybranowski S, Foster C, Wang S. Design of the First-in-Class, Highly Potent Irreversible Inhibitor Targeting the Menin-MLL Protein-Protein Interaction. *Angew Chem Int Ed Engl.* 2018;57(6):1601-1605.
37. Caswell R, Owens MO, Gunning AG, Ellard S, Wright CF. Data from: Thermodynamic analysis in silico of missense variants in MEN1. Figshare. Deposited 12 September 2019. <https://doi.org/10.1101/661512>.
38. The PyMOL Molecular Graphics System, Version 2.2. Schrödinger, LLC, 2018.
39. Kabsch W, Sander C. Dictionary of protein secondary structure: pattern recognition of hydrogen-bonded and geometrical features. *Biopolymers.* 1983; 22(12):2577-2637.

40. Touw WG, Baakman C, Black J, te Beek TA, Krieger E, Joosten RP, Vriend G. A series of PDB-related databanks for everyday needs. *Nucleic Acids Res.* 2015; 43(Database issue):D364-D368.
41. DSSP-3.0.0. Nijmegen, Netherlands: Centre for Molecular and Biomolecular Informatics, Radboud University Medical Centre, 2018. <https://swift.cmbi.umcn.nl/gv/dssp/index.html>
42. Tien MZ, Meyer AG, Sydykova DK, Spielman SJ, Wilke CO. Maximum allowed solvent accessibilities of residues in proteins. *PLoS One.* 2013;8(11):e80635.
43. Kozłowski LP, Bujnicki JM. MetaDisorder: a meta-server for the prediction of intrinsic disorder in proteins. *BMC Bioinformatics.* 2012;13:111. <http://genesilico.pl/metadisorder/>. Accessed December 31 2018.
44. Tate JG, Bamford S, Jubb HC, Sondka Z, Beare DM, Bindal N, Boutselakis H, Cole CG, Creatore C, Dawson E, Fish P, Harsha B, Hathaway C, Jupe SC, Kok CY, Noble K, Ponting L, Ramshaw CC, Rye CE, Speedy HE, Stefancsik R, Thompson SL, Wang S, Ward S, Campbell PJ, Forbes SA. COSMIC: the Catalogue Of Somatic Mutations In Cancer. *Nucleic Acids Res.* 2019, 47(D1):D941-D947.
45. Tokuriki N, Tawfik DS. Stability effects of mutations and protein evolvability. *Curr Opin Struct Biol.* 2009;19(5):596-604.
46. Shimazu S, Nagamura Y, Yaguchi H, Ohkura N, Tsukada T. Correlation of mutant menin stability with clinical expression of multiple endocrine neoplasia type 1 and its incomplete forms. *Cancer Sci.* 2011;102(11):2097-2102.
47. Canaff L, Vanbellinghen JF, Kanazawa I, Kwak H, Garfield N, Vautour L, Hendy GN. Menin missense mutants encoded by the *MEN1* gene that are targeted to the proteasome: restoration of expression and activity by CHIP siRNA. *J Clin Endocrinol Metab.* 2012;97(2):E282-291.
48. SIFT (Sorts Intolerant from Tolerant). La Jolla, CA: J. Craig Venter Institute. <http://provean.jcvi.org/index.php>. Accessed March 03 2019.
49. Adzhubei IA, Schmidt S, Peshkin L, Ramensky VE, Gerasimova A, Bork P, Kondrashov AS, Sunyaev SR. A method and server for predicting damaging missense mutations. *Nat Methods.* 2010;7(4):248-249. <http://genetics.bwh.harvard.edu/pph2/>. Accessed March 03 2019.
50. Ioannidis NM, Rothstein JH, Pejaver V, Middha S, McDonnell SK, Baheti S, Musolf A, Li Q, Holzinger E, Karyadi D, Cannon-Albright LA, Teerlink CC, Stanford JL, Isaacs WB, Xu J, Cooney KA, Lange EM, Schleutker J, Carpten JD, Powell IJ, Cussenot O, Cancel-Tassin G, Giles GG, MacInnis RJ, Maier C, Hsieh CL, Wiklund F, Catalona WJ, Foulkes WD, Mandal D, Eeles RA, Kote-Jarai Z, Bustamante CD, Schaid DJ, Hastie T, Ostrander EA, Bailey-Wilson JE, Radivojac P, Thibodeau SN, Whittemore AS, Sieh W. REVEL: An Ensemble Method for Predicting the Pathogenicity of Rare Missense Variants. *Am J Hum Genet.* 2016;99(4):877-885. <https://sites.google.com/site/revelgenomics/downloads>. Accessed March 03 2019.
51. Oza AM, DiStefano MT, Hemphill SE, Cushman BJ, Grant AR, Siegert RK, Shen J, Chapin A, Boczek NJ, Schimmenti LA, Murry JB, Hasadsri L, Nara K, Kenna M, Booth KT, Azaiez H, Griffith A, Avraham KB, Kremer H, Rehm HL, Amr SS, Abou Tayoun AN; ClinGen Hearing Loss Clinical Domain Working Group. Expert specification of the ACMG/AMP variant interpretation guidelines for genetic hearing loss. *Hum Mutat.* 2018;39(11):1593-1613.
52. Sivley RM, Dou X, Meiler J, Bush WS, Capra JA. Comprehensive Analysis of Constraint on the Spatial Distribution of Missense Variants in Human Protein Structures. *Am J Hum Genet.* 2018;102(3):415-426.

53. Landrum MJ, Lee JM, Benson M, Brown G, Chao C, Chitipiralla S, Gu B, Hart J, Hoffman D, Hoover J, Jang W, Katz K, Ovetsky M, Riley G, Sethi A, Tully R, Villamarin-Salomon R, Rubinstein W, Maglott DR. ClinVar: public archive of interpretations of clinically relevant variants. *Nucleic Acids Res.* 2016;44(D1):D862-D868.
54. Stein A, Fowler DM, Hartmann-Petersen R, Lindorff-Larsen K. Biophysical and Mechanistic Models for Disease-Causing Protein Variants. *Trends Biochem Sci.* 2019; 44(7):575-588.

Figure 1: Structure and disorder in menin. A) The structure of menin, as represented by PDB entry 3u88 chain A; protein surface is coloured from blue, N-terminal to red, C-terminal; the position of the binding pocket for JunD and KMT2A is indicated; numbered residues coloured magenta indicate positions flanking disordered loops which are not resolved in the crystal structure. B) menin (grey) in complex with KMT2A (yellow) and PSIP (green), as determined in PDB 3u88; note that while one end of KMT2A occupies the binding pocket, interaction with PSIP and other regions of KMT2A extends over a wider region of the menin surface. C) Probability of intrinsic disorder in menin, as calculated by the MetaDisorder predictor, plotted against amino acid position; extended regions of probability >0.5 are considered to be disordered. D) Coverage of menin residues in the 31 PDB structures used in this analysis, aligned against amino acid position as in part C. The top line shows coverage in PDB 3u88A, coloured as in 1A; numbering indicates residues flanking unstructured regions missing from the crystal structure. Below this, black horizontal lines show coverage for the 30 remaining PDB structures, while positions of benign and pathogenic variants are indicated by blue or red triangles indicate respectively. Note that regions of predicted intrinsic disorder are absent from the majority, if not all crystal structures, consistent with greater mobility of these residues within the crystal, and that few pathogenic variants have been reported in these regions.

Figure 2: Alignment of menin structures. A) The α carbon atoms of the 31 menin structures used in this study were aligned to that of PDB 6b41; each chain is shown in ribbon format, coloured by PDB and chain identifier; the position of the JunD/KMT2A binding pocket is indicated; the short helix visible at the top right of the rotated figure corresponds to residues 596-608 at the extreme C-terminal of menin, which were resolved only in PDB 3u84 chain A. B) As A, but superimposed with the structures of MLL (blue) and PSIP (grey) from PDB 3u88.

Figure 3: Pathogenic variants are predicted to destabilise menin structure. A) *In silico* mutagenesis and thermodynamic analysis for menin variants; for each variant, the average change in thermodynamic stability, $\Delta\Delta G$, was calculated across all structures contained the relevant residue, then plotted by variant group; black circles and vertical lines within each data area represent median and upper and lower quartiles respectively. Numbering above data points shows p values (Student's Two-tailed t-test) between groups as indicated. B) $\Delta\Delta G$ values for benign (blue) and pathogenic (red) variant groups calculated for 31 individual PDB structures as shown on the x-axis. C) Average $\Delta\Delta G$ values for benign and pathogenic variants occurring at the same amino acid position (residues with one benign and one pathogenic variant, $n=16$; residues with two benign and one pathogenic variants, $n=5$; residues with one benign and two pathogenic variants, $n=1$); coloured boxes show the range between upper and lower quartiles; horizontal lines within each data box show median value; data points are shown for outliers only. The difference in the average $\Delta\Delta G$ value between groups was highly significant ($p=0.0002$).

Figure 4: Population frequency of *MEN1* variants. The frequency of benign and uncertain missense variants in the gnomAD database plotted against $\Delta\Delta G$ value; blue fill: variants occurring in the gnomAD database only; yellow fill: variants reported in the gnomAD and SGCD databases; grey fill: variants in both gnomAD and HGMD Pro (DM class) databases. In cases where different nucleotide substitutions give rise to the same amino acid change, frequency is shown as a total for all variant alleles.

Figure 5: Molecular distribution of pathogenic and benign variants. A) Relative solvent accessibility was calculated for each variant group; black circles and vertical lines within each data area represent median and upper and lower quartiles respectively. Numbering above data points shows p values (Student's Two-tailed t-test) between groups as indicated. B) Buried pathogenic variants are predicted to be the most destabilising to menin structure; note that 6/7 of the novel missense variants reported here are deeply buried within the protein ($RSA < 0.02$), while only novel variant H46P is solvent accessible. C, D) Surface distribution of solvent-accessible variants. The surface of menin (grey), either alone (C) or in complex (D) with KMT2A (yellow) and PSIP (green) shows all variants with $RSA > 0.2$: blue, benign; red, pathogenic; purple colouring show positions at which different pathogenic and benign variants have been observed; the novel H46P variant is coloured cyan. The broken yellow oval indicates a cluster of pathogenic variants which may constitute an as yet unidentified interface for protein-protein interactions. E) menin is shown as a grey ribbon; novel missense variants are coloured cyan with sidechains displayed in stick format; KMT2A and DSIP are shown as in D.

Figure 6: Effect of protein-protein interaction on $\Delta\Delta G$. Analysis of solvent accessibility and thermodynamic effect of variants was performed on PDB 3u88 (menin:KMT2A:DSIP complex), both on menin chains in isolation (chains A, B) and as part of the complex. The upper graph shows the average difference in solvent accessibility by position in the complexed and isolated menin chains respectively ($\Delta RSA = RSA [\text{complex}] - RSA [\text{isolated}]$); the lower graph shows the equivalent difference in average $\Delta\Delta G$ value at each position (i.e. $\Delta\Delta\Delta G$); data points are labelled for variants where $\Delta\Delta\Delta G \geq 3$ kcal/mol; background shading indicates positions of menin residues forming contacts with KMT2A (yellow) or DSIP (green) in PDB 3u88.

Figure 7. Predicted thermodynamic stability correlates with observed expression. A) Steady-state expression levels have been reported for a number of menin variants; relative expression level data was sorted into two groups according to $\Delta\Delta G$ value as calculated in this study (neutral or weakly destabilising: $\Delta\Delta G < 3$ kcal/mol [$n=14$]; strongly destabilising: > 3 kcal/mol [$n=27$]); boxes show the range between upper and lower quartiles; horizontal lines within each data box show median value; data points are shown for outliers only. The difference in relative expression between the two groups was highly significant ($p=0.0001$).

Figure 8. Using thermodynamic analysis to assess the impact of novel missense variants. A) ROC curves for groups of pathogenic and benign variants as functions of $\Delta\Delta G$ value (red line; AUC, 0.833), REVEL score (blue line; AUC, 0.864) PolyPhen2 probability for pathogenicity (black line; AUC, 0.819) and SIFT score (broken black line; AUC = 0.819); open circles on $\Delta\Delta G$ and REVEL traces indicate positions corresponding to threshold values of 3 kcal/mol and 0.7 respectively. B) Scatter plot of $\Delta\Delta G$ value against REVEL score for all variants (red circles, pathogenic; blue fill, benign; grey fill, uncertain; cyan fill, novel). Where different nucleotide substitutions give rise to the same amino acid change, the REVEL score was calculated as an average of values for the individual nucleotide variants. Broken

horizontal and vertical lines indicate thresholds of $\Delta\Delta G = 3$ kcal/mol and REVEL score = 0.7 respectively; note that all 7 novel missense variants cluster in the upper right quadrant of the plot.

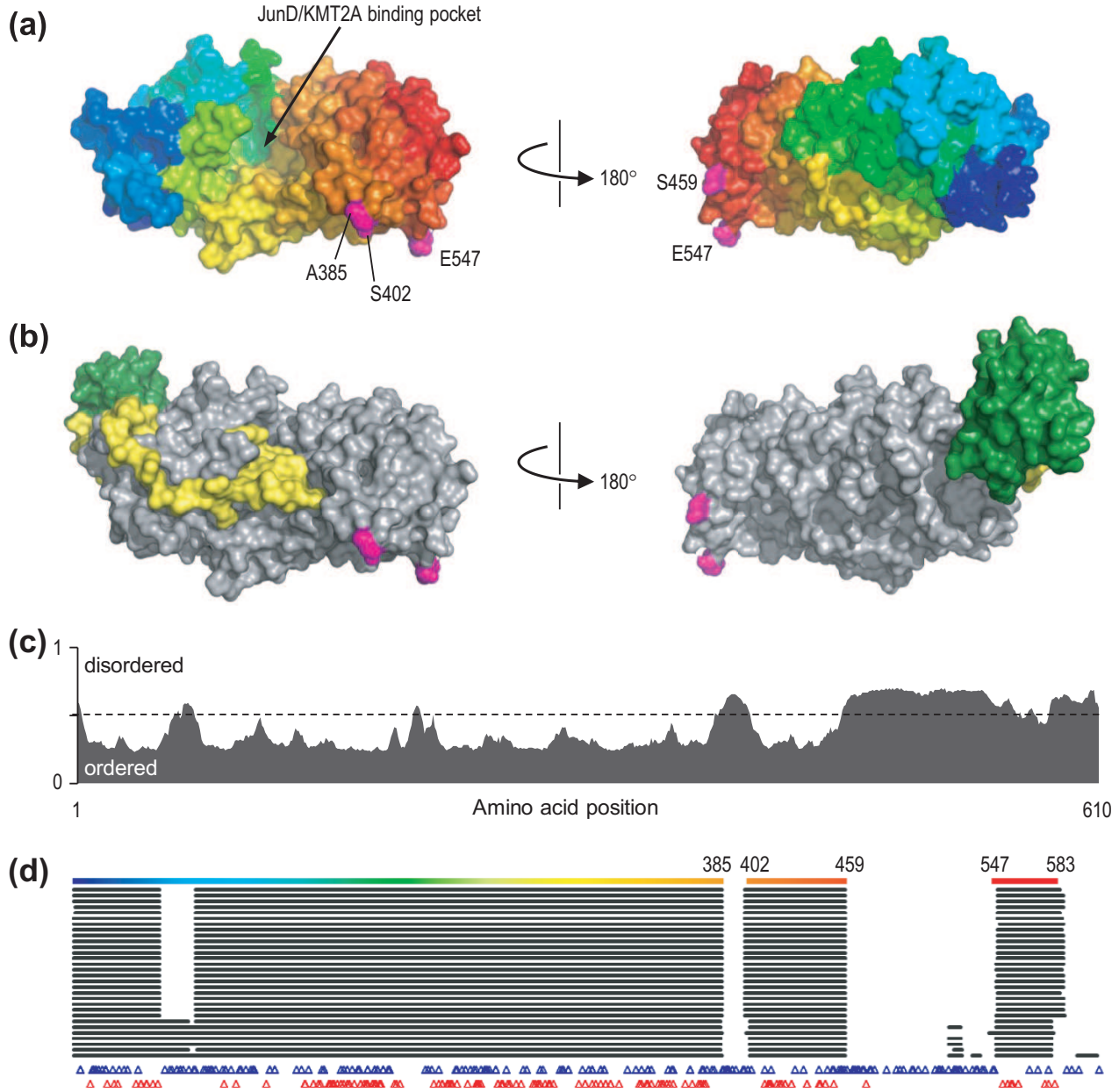
Table 1: Details of 7 novel missense variants in *MEN1*. All variants refer to *MEN1* transcript NM_130799.2, protein NP_570711.1 (610 amino acid isoform).

| variant # | 1 | 2 | 3 | 4 | 5 | 6 | 7 |
|-------------------------------|-------------------|-------------------|-------------------|-------------------|-------------------|-------------------|-------------------|
| HGVS c. notation | c.137A>C | c.490G>C | c.524T>C | c.1033G>C | c.1078A>T | c.1091T>C | c.1256G>A |
| HGVS p. notation | p.(His46Pro) | p.(Ala164Pro) | p.(Leu175Pro) | p.(Ala345Pro) | p.(Ile360Phe) | p.(Phe364Ser) | p.(Gly419Asp) |
| genomic variant (GRCh37/hg19) | chr11:64577445T>G | chr11:64575527C>G | chr11:64575493A>G | chr11:64573720C>G | chr11:64573214T>A | chr11:64573201A>G | chr11:64572600C>T |
| reported in gnomAD? | no | no | no | no | no | no | no |
| SIFT prediction | Damaging | Damaging | Damaging | Damaging | Damaging | Damaging | Damaging |
| PROVEAN prediction | Deleterious | Deleterious | Deleterious | Deleterious | Deleterious | Deleterious | Deleterious |
| PolyPhen prediction | probably damaging | probably damaging | probably damaging | probably damaging | probably damaging | probably damaging | probably damaging |
| REVEL score | 0.894 | 0.925 | 0.965 | 0.909 | 0.883 | 0.945 | 0.912 |

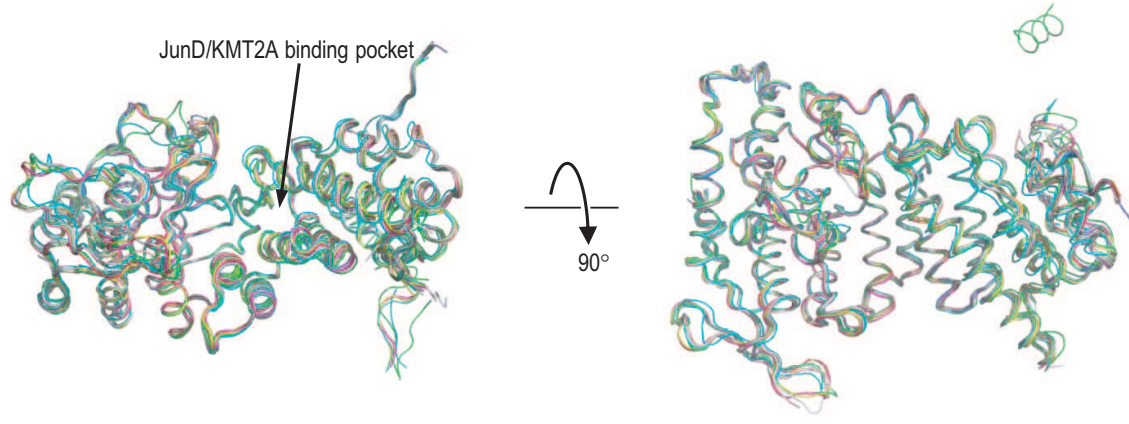
Table 2: *MEN1* crystal structures used in FoldX analysis. A total of 29 PDB structures containing 31 menin chains were used for thermodynamic analysis using FoldX; 7 representative structures were also used for relative solvent accessibility (RSA) analysis.

| PD B ID | Title | resolution (Å) | release date | Menin chain(s) | used for RSA analysis? | Reference |
|---------|--|----------------|--------------|----------------|------------------------|-----------|
| 3u84 | Crystal structure of Human Menin | 2.50 | 15/02/2012 | A, B | Yes (chain A) | 29 |
| 3u85 | Crystal structure of human menin in complex with MLL1 (KMT2A) | 3.00 | 15/02/2012 | A | Yes | |
| 3u86 | Crystal structure of human menin in complex with JunD | 2.84 | 15/02/2012 | A | | |
| 3u88 | Crystal structure of human menin in complex with MLL1 (KMT2A) and LEDGF (PSIP) | 3.00 | 15/02/2012 | A, B | Yes (chain B) | |
| 4gpq | Structural insights into inhibition of the bivalent menin-MLL interaction by small molecules in leukemia | 1.46 | 19/09/2012 | A | | 30 |
| 4gq3 | Human menin with bound inhibitor MI-2 | 1.56 | 19/09/2012 | A | | |
| 4gq4 | Human menin with bound inhibitor MI-2-2 | 1.27 | 19/09/2012 | A | | |
| 4gq6 | Human menin in complex with MLL (KMT2A) peptide | 1.55 | 19/09/2012 | A | | |
| 4i80 | Crystal structure of human menin in complex with a high-affinity macrocyclic peptidomimetics | 3.10 | 06/03/2013 | A | Yes | 31 |
| 4og3 | Human menin with bound inhibitor MIV-3R | 2.01 | 05/03/2014 | A | | 32 |
| 4og4 | Human menin with bound inhibitor MIV-3S | 1.45 | 05/03/2014 | A | | |
| 4og5 | Human menin with bound inhibitor MIV-5 | 1.63 | 05/03/2014 | A | | |
| 4og6 | Human menin with bound inhibitor MIV-4 | 1.49 | 05/03/2014 | A | | |
| 4og7 | Human menin with bound inhibitor MIV-7 | 2.08 | 05/03/2014 | A | | |
| 4og8 | Human menin with bound inhibitor MIV-6R | 1.53 | 05/03/2014 | A | | |
| 4x5y | Menin in complex with MI-503 | 1.59 | 15/04/2015 | A | | 33 |
| 4x5z | Menin in complex with MI-136 | 1.86 | 15/04/2015 | A | | |
| 5db0 | Menin in complex with MI-352 | 1.50 | 30/03/2016 | A | | 34 |

| | | | | | | |
|----------|------------------------------|------|----------------|---|-----|----|
| 5db 1 | Menin in complex with MI-336 | 1.86 | 30/03/20 16 | A | | 35 |
| 5db 2 | Menin in complex with MI-389 | 1.54 | 30/03/20 16 | A | | |
| 5db 3 | Menin in complex with MI-574 | 1.71 | 30/03/20 16 | A | | |
| 5dd 9 | Menin in complex with MI-326 | 1.62 | 09/09/20 15 | A | | |
| 5dd a | Menin in complex with MI-333 | 1.83 | 09/09/20 15 | A | Yes | |
| 5dd b | Menin in complex with MI-319 | 1.54 | 09/09/20 15 | A | | |
| 5dd c | Menin in complex with MI-2-3 | 1.62 | 06/07/20 16 | A | | |
| 5dd d | Menin in complex with MI-836 | 2.14 | 09/09/20 15 | A | | |
| 5dd e | Menin in complex with MI-859 | 1.78 | 09/09/20 15 | A | | |
| 5dd f | Menin in complex with MI-273 | 1.66 | 09/09/20 15 | A | Yes | 36 |
| 6b4 1 | Menin bound to M-525 | 2.61 | 24/01/20 18 | A | Yes | |



(a)



(b)

